Multicell converters

Guillaume Gateau, Maurice Fadel, Pascal Maussion, Rédha Bensaid, Thierry A Meynard

Multicell Converters: Active Control and Observation of Flying-Capacitor Voltages

Guillaume Gateau, Maurice Fadel, Pascal Maussion, Rédha Bensaid, and Thierry A. Meynard, *Member, IEEE*

***Abstract*—The multicell converters introduced more than ten years ago make it possible to distribute the voltage constraints among series-connected switches and to improve the output waveforms (increased number of levels and apparent frequency). The balance of the constraints requires an appropriate distribution of the flying voltages. This paper presents some solutions for the active control of the voltages across the flying capacitors in the presence of rapid variation of the input voltage. The latter part of this paper is dedicated to the observation of these voltages using an original modeling of the converter.**

***Index Terms*—Kalman filtering, multilevel systems, nonlinear systems, power electronics, power systems harmonics.**

I. Introduction

INCREASING the power of the static converters is generally obtained by increasing the voltage because of efficiency requirements. For example, industrial applications with power of a few megawatts generally use voltages of several kilovolts. The static converters should follow the same rule, but medium-voltage switching devices are not available. The tradeoff between efficiency, waveform purity, and volume of the converter and of corresponding filters must also be carefully studied. In this logic, the studies and development carried out on the capacitor clamped multicell converters over the past ten years revealed excellent characteristics regarding the previous criteria. Indeed, this type of structure makes it possible to split the voltage constraints and to distribute them on several switches of smaller ratings in series. These structures also make it possible to obtain a significant improvement of the output waveforms and to increase the apparent frequency of this wave, allowing a significant reduction of the filtering elements. This type of converter uses flying capacitors to split the input voltage and the evolution of their voltages must be carefully studied since the survival of the converter depends on it.

Many studies [1], [3], [5], [7] have shown that, under certain conditions, a simple open-loop control guarantees natural balancing of the flying voltages. Nevertheless, in this case, the dynamics involved in the balancing transient depend on the impedance of load at the switching frequency. If the impedance at the switching frequency is high (small current harmonic at this frequency) then the natural balancing is very slow and inversely. This observation has allowed the development of solutions based on an extra "balance booster" which is a simple *RLC* circuit with a natural frequency equal to the switching frequency [5], [8]. However, although the dynamics of rebalancing are really improved, they t may still be too slow to follow rapid variations of the input voltage.

All these observations lead us to propose solutions for an active control of the flying voltages. This control can be carried out in duration (duty cycle [5]) or in amplitude (sliding mode [10]).

Section II of this paper will be dedicated to modeling of the converter. Then, in Section III, we will present a synthesis of control strategies based on the theoretical principle of input/output linearization. In Section IV, we will tackle the problem of the observation of the flying-capacitor voltages by using an original model of the converter sampled at p times the switching frequency if the number of cells is p. We will give finally some conclusions on this work in Section V.

II. Modelization of Multicell Converters

Modeling represents an essential part in the study of a control strategy for a given converter. In power electronics, we often use a model with the instantaneous average values while shifting the average value over one switching period. The case of the multicell converter is a little particular because the generation of harmonics at the switching frequency contributes to the natural balancing of the flying capacitor voltages [1]. In this case, the average model does not make it possible to represent the natural dynamics of balancing of the flying capacitor voltages. However, this phenomenon remains generally rather slow and can be easily neglected when using active regulation of the voltages.

A. Instantaneous Model of the Converter

The topology of the converter being variable, its operation can be described by a set of state equations corresponding to the various electric configurations established during one period of operation.

With p commutation cells, each one having two possible states, we have $2 \times p$ possible configurations. The control signal associated with each commutation cell is noted as u_i where i represents the number of cells of the topology. This signal will be equal to 1 when the upper switch of the cell is conducting and 0 when the lower switch of the cell is conducting.

Fig. 1 represents a three-cell chopper associated with a load formed by a resistor R and an inductor L.

From the circuit equations, it is possible to write in this case three differential equations (1) representing the evolution of the

Manuscript received July 19, 2001; revised November 30, 2001. Abstract published on the Internet July 15, 2002.

The authors are with the Laboratoire d'Electrotechnique et d'Electronique Industrielle, Institut National Polytechnique de Toulouse/Centre National de la Recherche Scientifique, 31071 Toulouse Cedex 7, France (e-mail: gateau@leei.enseeiht.fr; meynard@leei.enseeiht.fr).

Publisher Item Identifier 10.1109/TIE.2002.803200.

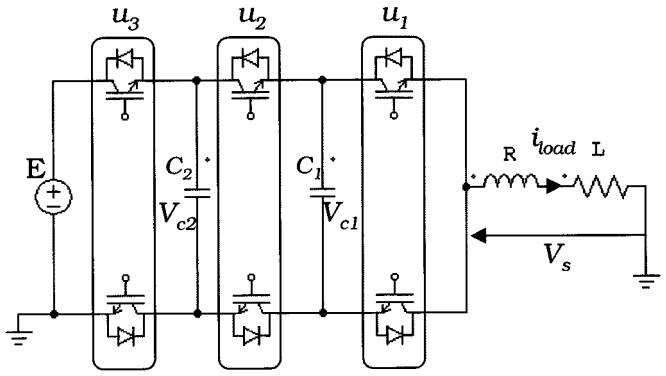

Fig. 1. Three-cell chopper.

three state variables of the converter, namely, the two flying capacitor voltages as well as the current in the load

$$\begin{cases} \dot{v_{c1}} = \dot{x_1} = -\frac{1}{C_1} x_3 (u_1 - u_2) \\ \dot{v_{c2}} = \dot{x_2} = -\frac{1}{C_2} x_3 (u_2 - u_3) \\ \dot{i_{\text{load}}} = \dot{x_3} = -\frac{R}{L} x_3 + \frac{1}{L} Vs \end{cases} \tag{1}$$

with $\boldsymbol{U} = (u_1, u_2, u_3)^t$ representing the state of the commutation cells and $\boldsymbol{X} = (x_1, x_2, x_3)^t$ the state vector of the system.

This model is the instantaneous model of the converter and can be used for any purpose such as simulation or control of the converter. It can be used also for studying the natural balancing phenomena of the flying-capacitor voltages.

B. Affine Representation of the Model

It is possible to put the differential equations of the system in an affine linear form in order to apply thereafter the theory of input–output linearization. For this purpose, we use the average model over one switching period for all the state variables and the control input. It is then possible to rewrite the equations as follows:

$$\begin{cases} \dot{X} = f(X) + G(X)U = AX + \sum_{i=1}^{p} g_i(X) u_i \\ y = h(X) \end{cases} \tag{2}$$

with

$$\begin{cases} f(x) = \left[0, 0, -\frac{R}{L}\right]^t \\ G(x) = \begin{bmatrix} -\frac{x_3}{C_1} & \frac{x_3}{C_1} & 0 \\ 0 & -\frac{x_3}{C_2} & \frac{x_3}{C_2} \\ \frac{x_1}{L} & \frac{(x_2 - x_1)}{L} & \frac{(E - x_2)}{L} \end{bmatrix} \\ h(X) = I_3 X, \qquad \text{with } I_3 = \text{identity matrix.} \end{cases} \tag{3}$$

These equations enable us to highlight the nonlinear form of the converter. These nonlinearities are present mainly in matrix $G(X)$.

III. Control of Multicell Converters

The main objective of the active control of the converter is multiple: obviously, we have to control the output current but we also have to control the voltages across the flying capacitors. Indeed, even if many studies have shown that the flying-capacitor voltages are balanced in a natural way when the duty cycles are equal with a phase shift of $2\pi/p$ (where p is the number of cells), the dynamics of balancing remain slow. For this reason, we propose an active control of the flying-capacitors voltages which will allow the converter to follow fast variations of the input voltage.

A. Nonlinear Control by Input–Output Linearization

We initially wish to obtain a complete linearization of the system. In the second pass, we will carry out the regulation of the state variables by using a linear synthesis. Decoupling enables us to associate a control input to each state variable. Each control input thus becomes dedicated to one and only one state variable and the action on this control input does not modify the other state variables.

The linearization of the system is obtained by an algebraic transformation described in [11]–[13]. It uses a new input v of the system defined by (4)

$$u(X) = \alpha(X) + \beta(X) v \tag{4}$$

with

$$\begin{cases} \alpha(X) = -\Delta^{-1}(X)\Delta_0(X) \\ \beta(X) = \Delta^{-1}(X) \\ \text{and v is the new input.} \end{cases}$$

The definition of this new input vector is, thus, carried out by using a decoupling matrix $\Delta(x)$ as well as a vector $\Delta_0(x)$ defined, respectively, by (5) and (6), shown at the bottom of the page, where $L_f h_j(X)$ is the Lie derivative of h_j over f, and m is the number of inputs. Fig. 2 represents the nonlinear linearization of the system with the definition of the new input vector v.

The result of this exact linearization corresponds to p integrators (where p is the number of cells), each one controlled by an input as shown in Fig. 3. It will be necessary to provide a second linear loop in order to set the dynamic on each state variable.

$$\Delta(X) = \begin{pmatrix} L_{g_1} L_f^{(r_1 - 1)} h_1(X) & \cdots & L_{g_m} L_f^{(r_1 - 1)} h_1(X) \\ \vdots & \ddots & \vdots \\ L_{g_1} L_f^{(r_m - 1)} h_m(X) & \cdots & L_{g_m} L_f^{(r_m - 1)} h_m(X) \end{pmatrix} \tag{5}$$

$$\Delta_0(X) = \begin{pmatrix} L_f^{(r_1)} h_1(X) \\ \vdots \\ L_f^{(r_m)} h_m(X) \end{pmatrix} \tag{6}$$

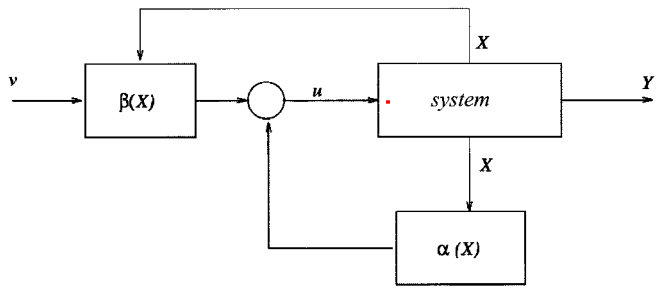

Fig. 2. Representation of input–output linearization principle.

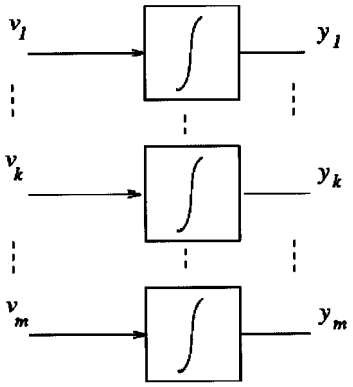

Fig. 3. System after input–output linearization.

B. Application of Input–Output Linearization on Three-Cell Converter

In the case of the state equations given in (2) and (3), we obtain after calculation the decoupling matrices given in (7)

$$\begin{cases} \beta(X) = \begin{bmatrix} \frac{C_1(x_1-E)}{E\times x_3} & \frac{C_2(x_2-E)}{E\times x_3} & \frac{L}{E} \\ \frac{(x_1)}{E\times x_3} & \frac{C_2(x_2-E)}{E\times x_3} & \frac{L}{E} \\ \frac{(x_1)}{E\times x_3} & \frac{(x_2)}{E\times x_3} & \frac{L}{E} \end{bmatrix}^t \\ \alpha(X) = -\Delta(X)^{-1}\Delta_0(X) = -R\frac{x_3}{E}\begin{bmatrix} 1 \\ 1 \\ 1 \end{bmatrix}. \end{cases} \tag{7}$$

As we can note, the decoupling of the system reveals two singularities, one when the input voltage is equal to zero and the other when the output current is null. These two singularities correspond to the fact that, in these cases, the control of the flying capacitors voltages is not possible.

The problem of the zero crossing of the input voltage will be solved simply by supposing that, for such a system, we always work with an input voltage greater than 0.

The problem of the current will be solved by blocking the linearization in the vicinity of zero current. This will disturb slightly the dynamic, since in this point the evolution is proportional to the current amplitude, which means a very slow evolution for low current.

After the realization of the input–output linearization based on Fig. 2, it is necessary to control the state variables by using the new uncoupled model of the system represented in Fig. 3.

C. Proportional Regulation of State Variable

We initially present the choice of a simple proportional regulation as represented in Fig. 4 and where X_{ref} is a vector composed by the reference for each state variable. A simple proportional regulation is normally sufficient and must make it possible to obtain a null static error in steady state because we obtain after decoupling a system with a natural integration as shown in Fig. 3.

The choice of the proportional constant is carried out by fixing a closed-loop dynamic for the system. The transfer function in closed loop is given by (8)

$$T_{BF(s)} = \frac{1}{1+\frac{s}{K_p}} \tag{8}$$

with s being the Laplace variable and K_p the proportional action of the corrector.

The proportional action K_p should not be selected too large to avoid the saturation of the control signal. For the validation of this control strategy we simulated a three-cell converter having the following parameters:

$$\begin{cases} L = 1\text{ mH} \\ R = 10\,\Omega \\ Td = 62.5\ \mu\text{s (switching period)} \\ C_1 = C_2 = 40\ \mu\text{F} \\ K_{p1} = K_{p2} = K_{p3} = 5000 \\ r_e = 0.6\,\Omega \\ L_e = 1\text{ mH} \\ C_e = 500\ \mu\text{F (input filter)}. \end{cases}$$

The test cycle imposed on the state variables is as follows:

- $t = 0$—start reference current with 80 A;
- $t = 10$ ms—variation of -60 A for I_{ref};
- $t = 15$ ms—variation of $+60$ A for I_{ref};
- $t = 15$ ms—sinusoidal perturbation of E (300 V).

The simulation gives very good results as shown in Fig. 5. The current response is very fast and the tracking of the flying-capacitor voltages reference is very good.

It should be noted that the decoupling of the state variables is correct and, thus, that the variation of one state variable does not influence the other.

For the study of the saturation phenomena of the duty cycle limited between 0 and 1, we have to carry out a test cycle under weak load of the following:

- $t = 0$—start reference current with 80 A;
- $t = 10$ ms—variation of -70 A for I_{ref};
- $t = 10$ ms—variation of -200 V for input voltage.

The results shown in Fig. 6 are very good for load current and flying capacitors voltages, even if we can see a small perturbation at $t = 20$ ms due to the saturation of the duty cycle.

Fig. 7 shows the three duty cycles applied to the converter. The first part of the trial is similar to the results obtained on Fig. 5. However, at $t = 20$ ms, the reference of the current takes a very low value and we impose a variation of the input voltage. As we can see in this figure, the duty cycles are saturated and the result is a small perturbation on the current (shown in Fig. 6).

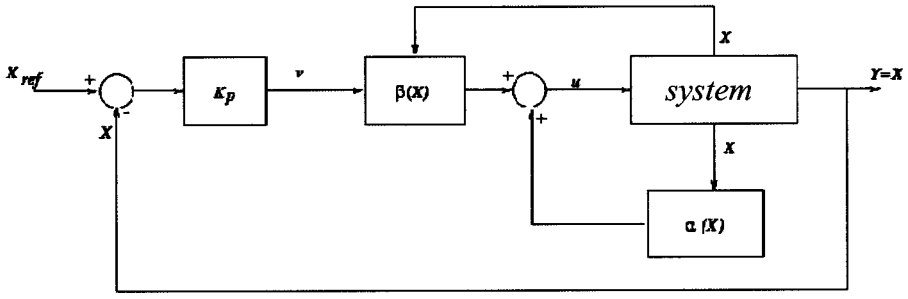

Fig. 4. Regulation loop for proportional regulator.

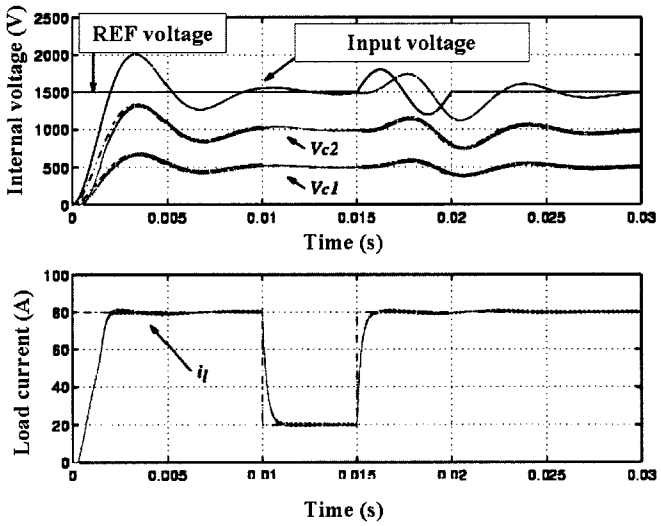

Fig. 5. Simulation results for voltages and current with proportional regulator.

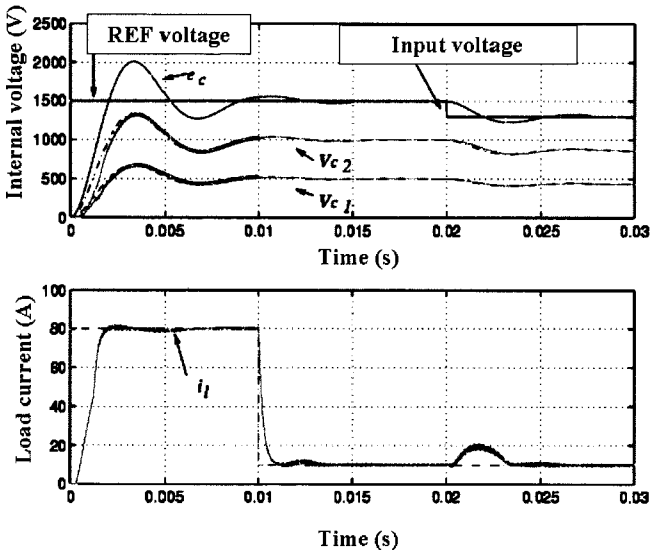

Fig. 6. Simulation results with duty-cycle saturation.

D. Integral Proportional (IP) Regulation of State Variables

The decoupling of the state variables leads to a linear system made of simple integrators. In the case of variable or badly identified parameters, these integrators are transformed into first

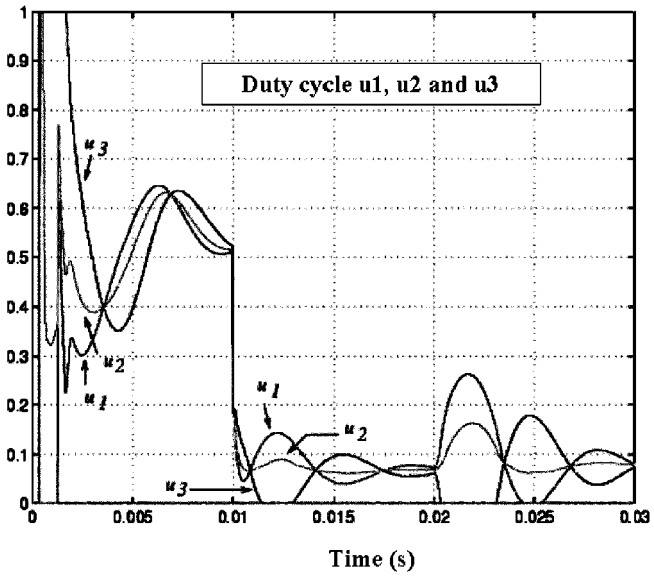

Fig. 7. Simulation results with duty-cycle saturation.

order systems, not revealing directly an integration and whose form (gain and dynamics) depends on the parametric error. To solve this problem, it is possible to add to the corrector an integral factor. This addition can be carried out by choosing a PI or IP corrector.

According to the observation of our decoupling struture, it appears more judicious to use a IP regulation as shown in Fig. 8, even if the adjustment of the corrector parameters cannot be made in an independent way.

For the choice of the parameters, it is necessary to write the closed-loop function (9) and to identify it with a classical second-order system with known damping and pulsation

$$T_{BF(s)} = \frac{1}{\tau_k \tau_{\text{int}} s^2 + 2\tau_{\text{int}} s + 1} \tag{9}$$

with s the Laplace variable and $\tau_k = 1/K_p$.

The parameters of the converter and the control law are given in (10)

$$\begin{cases} L = 1 \text{ mH}, R = 10\,\Omega \\ Td = 62.5\ \mu\text{s (switching period)} \\ C_1 = C_2 = 40\ \mu\text{F} \\ K_{p_1} = K_{p_2} = K_{p_3} = 5000 \\ \tau_{\text{int}} = 550\ \mu\text{s}. \end{cases} \tag{10}$$

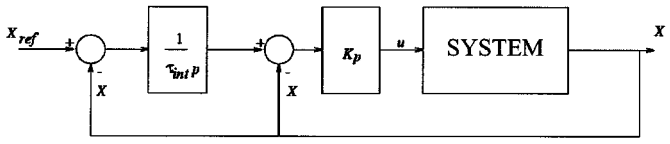

Fig. 8. Regulation loop with IP regulator.

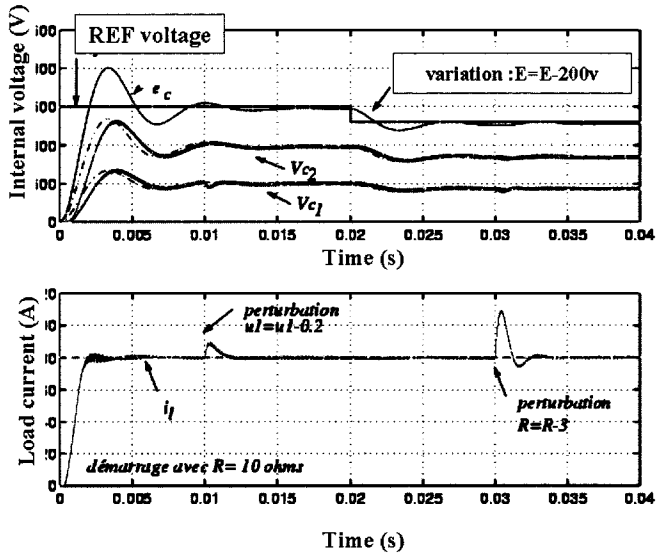

Fig. 9. Simulation results for current and voltages with IP regulator.

The test cycle will be as follows:

- $t = 0$—start reference current with 80 A;
- $t = 10$ ms—perturbation on control signal u_1;
- $t = 10$ ms—load variation (3 Ω).

Figs. 8 and 9 show very good results when starting the converter as well as during the perturbations applied to the system.

At $t = 10$ ms, the disturbance carried out on control input u_1 (shown in Fig. 9) is compensated quickly by the integral and the output current is only slightly disturbed (Fig. 8).

In order to validate this control law experimentally, we built a control unit based on a digital signal processor (DSP) to control a three-cell chopper. The parameters of the experimental model are the same as given in (10).

Fig. 10 shows the flying-capacitors voltages as well as the input voltage and Fig. 11 corresponds to the load current. It should be noted that the results are completely satisfactory and in conformity with the forecasts.

The balancing of the flying capacitors voltages is obtained in approximately 2 ms and induces a slight disturbance of the current for this period, as shown in Fig. 11. At $t = 2$ ms, the voltages across the capacitors are well balanced, and even if we applied large transient on the output current, these voltages would be very well controlled. Fig. 12 displays experimental results obtained with this setup.

IV. Observation of the Flying Capacitor Voltages

As shown before, an active control of the flying-capacitor voltages requires the knowledge of the state.

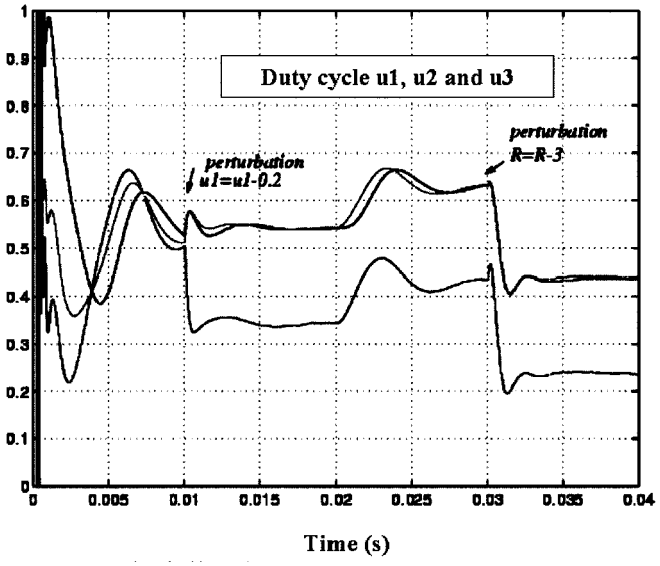

Fig. 10. Simulation results: duty cycle with IP regulator.

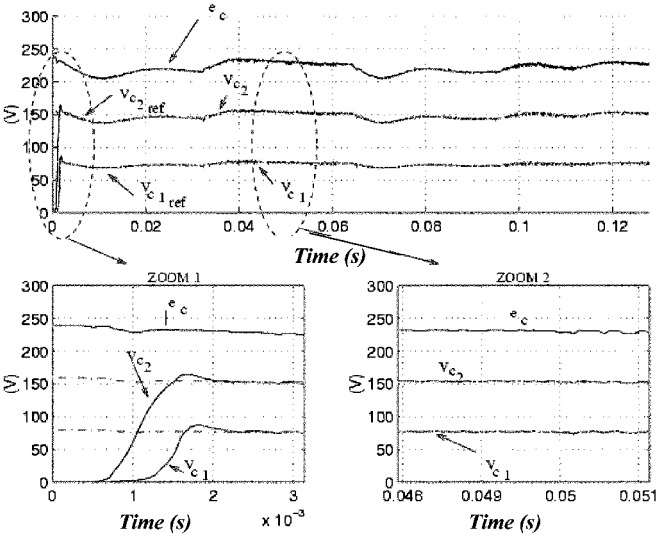

Fig. 11. Experimental results: capacitors voltage with IP regulator.

Usually, differential voltage sensors are used to measure the capacitor voltages, but the presence of these sensors increases the drive cost and size. As an example, the control of a three-cell three-phase inverter requires, at least, six floating voltage sensors plus two current sensors. Furthermore, in high-voltage applications, the design of the voltage sensors is not simple and usually requires a good insulation quality.

In order to reduce these sensors, several solutions are available and have been tested.

The first one is very simple and needs only one voltage sensor. Its basic principle consists of the measurement of the converter output voltage each time the input control vector changes. Thus, using the switches state information, one can easily find the capacitor and the supply voltages by resolving a linear algebraic equation system [5]. Obviously, this method does not correspond to a state observation since the system dynamics are not considered.

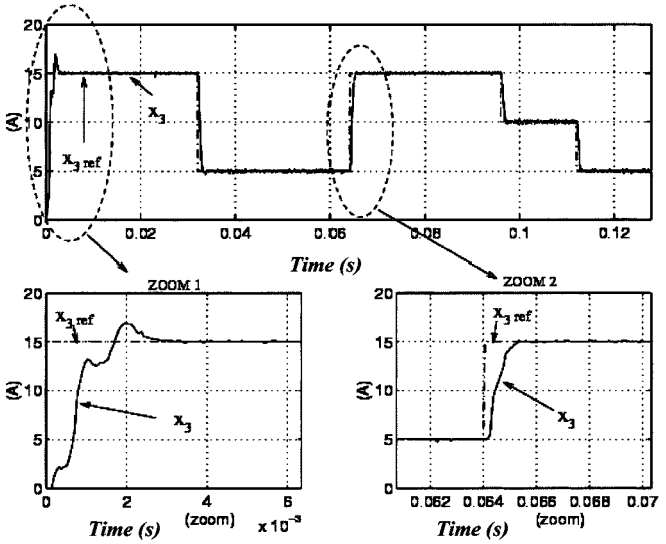

Fig. 12. Experimental results: load current with IP regulator.

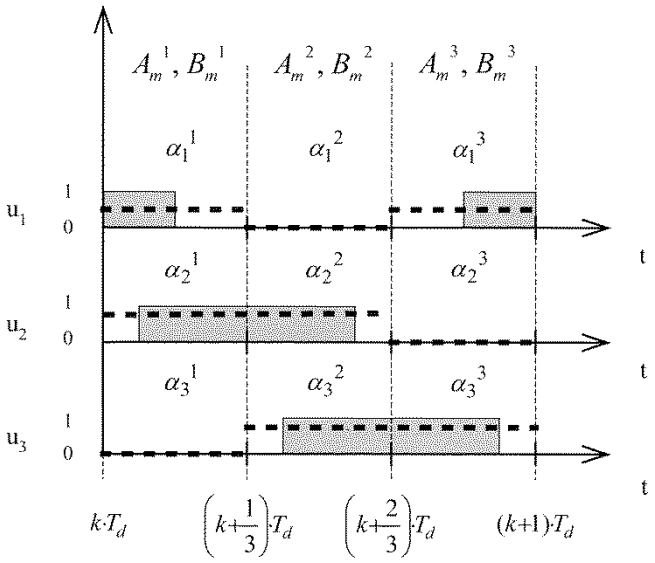

Fig. 13. Control signals respresentation and their average over one-third switching period.

The major drawback of this estimation technique is due to its high measurement noise sensitivity since any perturbation on the measurement is directly transposed to the estimated state and cannot be filtered by the system dynamics.

The second solution is to develop a state observer using a load current measurement. For this purpose, a good model representation of the system must be adopted. One can plan to use an exact discrete-time model of the converter, but this solution leads to a heavy computational load and consequently remains complex for a real-time implementation [15].

On the other hand, the classical average model is not precise enough and does not satisfy the observability condition when only the load current is measured.

In this paper, a novel and simple model based on average values over *one-third of switching period* is presented. We will show that this model represents sufficiently well the behavior of the converter and the capacitor voltages remain observable even if the natural balancing dynamics are not correctly represented.

A development of a discrete-time Kalman filter (KF) for the capacitor voltages estimation is then proposed. This structure of observer is actually well adapted since it takes into account the noise phenomena really present. Simulation and experimental results using a sensorless control strategy are presented to validate the observer.

A. Average Model Over One-Third Switching Period

In this section, a simple discrete-time model based on a state average technique is obtained for a three-cell chopper (Fig. 1). In the following, we assume a fixed switching period T_d and suppose that all switches are perfect. We also assume that the duty cycles and the source voltage E remain constant during the time interval $[kT_d, (k+1)T_d]$.

The instantaneous model of the chopper in the state-space representation can be described by the following:

$$\begin{cases} \dot{\mathbf{x}} = \mathbf{A}(\mathbf{u}) \cdot \mathbf{x} + \mathbf{B}(\mathbf{u}) \cdot E \\ y = \mathbf{C} \cdot \mathbf{x} \end{cases} \tag{11}$$

where

$$\mathbf{A}(\mathbf{u}) = \begin{bmatrix} 0 & 0 & \frac{u_2-u_1}{C_1} \\ 0 & 0 & \frac{u_3-u_2}{C_2} \\ \frac{u_1-u_2}{L_l} & \frac{u_2-u_3}{L_l} & -\frac{R_l}{L_l} \end{bmatrix}$$

$$\mathbf{B}(\mathbf{u}) = \begin{bmatrix} 0 \\ 0 \\ \frac{u_3}{L_l} \end{bmatrix}$$

$\mathbf{C} = [0 \quad 0 \quad 1]$, $\mathbf{x} = (v_{C_1}, v_{C_2}, i_L)^t$ E the input voltage source $\mathbf{u} = (u_1, u_2, u_3)^t$ the control signal vector, and $y = i_L$ is the measured state (observer input) and correspond to the load current.

The average model over $T_d/3$ is then obtained by replacing the instantaneous variables in (1) by their average values over *one-third period* ($T_d/3$). Of course, this is valid only if the time constants of the system are much larger than $T_d/3$ [18].

Thus, on the time interval $[kT_d, (k+1)T_d$, we calculate three new duty-cycle vectors $\alpha^j = (\alpha_1^j, \alpha_2^j, \alpha_3^j)^T_{(j=1\cdots3)}$ which represent the average of the control signals $u_{i=1\cdots3}$ over each interval of $T_d/3$ duration (Fig. 13)

$$\alpha_i^j = \langle u_i \rangle_{T_d/3} = \frac{3}{T_d} \int_{(j-1)T_d/3}^{j \cdot T_d/3} u_i dt, \qquad i,j = 1 \cdots 3. \tag{12}$$

We then obtain three continuous models per switching period T_d

$$\langle \dot{\mathbf{x}} \rangle^j = \mathbf{A}_m^j \cdot \langle \mathbf{x} \rangle^j + \mathbf{B}_m^j \cdot E, \qquad j = 1 \cdots 3 \tag{13}$$

where

$$\mathbf{A}_m^j = \begin{bmatrix} 0 & 0 & \frac{\alpha_2^j-\alpha_1^j}{C_1} \\ 0 & 0 & \frac{\alpha_3^j-\alpha_2^j}{C_2} \\ -\frac{\alpha_2^j-\alpha_1^j}{L_l} & -\frac{\alpha_3^j-\alpha_2^j}{L_l} & -\frac{R_l}{L_l} \end{bmatrix}$$

$$\mathbf{B}_m^j = \begin{bmatrix} 0 \\ 0 \\ \frac{\alpha_3^j}{L_l} \end{bmatrix}, \qquad \text{where } j = 1 \ldots 3.$$

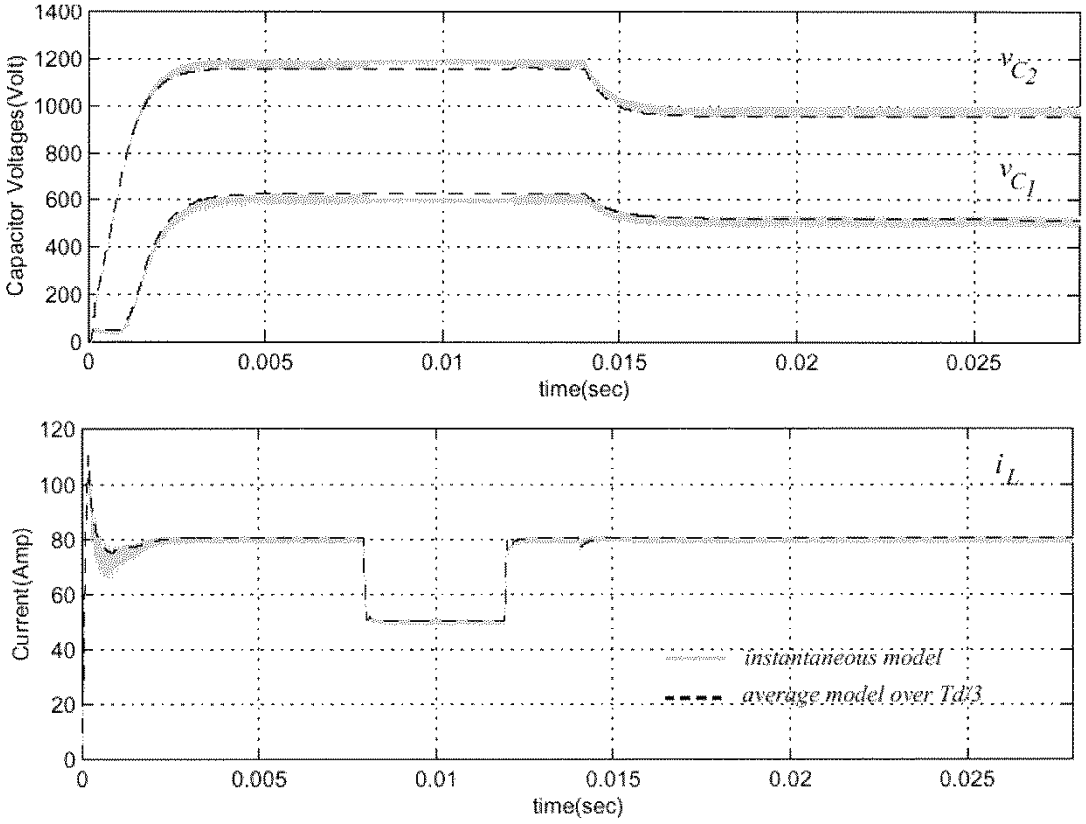

Fig. 14. Validation of the average model over one-third switching period.

Thereafter, these models are sampled with a period of $T_d/3$ using a second-order approximation to obtain three discrete-time equations per switching period, expressing the state at time $(k+j/3)\cdot T_d$ according to the state at time $(k+(j-1)/3)\cdot T_d$

$$\mathbf{x}\left(k+\frac{j}{3}\right)=\mathbf{F}_m^j\cdot\mathbf{x}\left(k+\frac{(j-1)}{3}\right)+\mathbf{G}_m^j\cdot E(k)\,(j=1\cdots3) \quad (14)$$

where

$$\begin{cases}\mathbf{F}_m^j=e^{\left(\mathbf{A}_m^j\right)\cdot T_d/3}\approx\mathbf{I}+\left(\mathbf{A}_m^j\right)\cdot\frac{T_d}{3}+\left(\mathbf{A}_m^j\right)^2\cdot\frac{\left(\frac{T_d}{3}\right)^2}{2}\\ \mathbf{G}_m^j\approx\left(\frac{T_d}{3}I+\left(\mathbf{A}_m^j\right)\frac{\left(\frac{T_d}{3}\right)^2}{2}\right)\cdot\mathbf{B}_m^j.\end{cases} \quad (15)$$

Finally, a *global model*, sampled with a period of T_d is obtained from the preceding equations

$$\mathbf{x}(k+1)=\mathbf{F}_m(k)\cdot\mathbf{x}(k)+\mathbf{G}_m(k)\cdot E(k) \quad (16)$$

with

$$\begin{cases}\mathbf{F}_m=\mathbf{F}_m^3\mathbf{F}_m^2\mathbf{F}_m^1\\ \mathbf{G}_m=\mathbf{F}_m^3\mathbf{F}_m^2\mathbf{G}_m^1+\mathbf{F}_m^3\mathbf{G}_m^2+\mathbf{G}_m^3\end{cases}. \quad (17)$$

Note that, since $\mathbf{A}_m^j$ and $\mathbf{B}_m^j$ depend on the duty cycles applied to the converter, $\mathbf{F}_m$ and $\mathbf{G}_m$ are time varying in transient and, for simplicity, will be noted $\mathbf{F}_m(k)$ and $\mathbf{G}_m(k)$ instead of $\mathbf{F}_m(\alpha(k))$ and $\mathbf{G}_m(\alpha(k))$. In steady-state operation, the duty cycles are constant and the model is stationary.

B. Validation of the Model

The following simulation (Fig. 14) shows that the average model over $T_d/3$ represents correctly the behavior of the converter in the closed-loop operation. The control strategy used for this simulation is the linear state feedback decoupling control [19] and the converter parameters are given in (10).

However, this model does not correctly represent the natural balancing of the capacitor voltages since many harmonics are lost when averaging the instantaneous model. Nevertheless, since the main goal of an observer design is to estimate the capacitor voltages for a closed-loop control use, we can neglect the natural balancing dynamics according to the desired closed-loop dynamics.

C. Discrete KF

In the last section, it has been assumed that the system can be represented perfectly by a deterministic state-space model (14). In practice, this is not the case, due to the presence of disturbances for which modeling would be difficult and result in complex equations.

For handling system uncertainties of this nature, a stochastic model is used. This stochastic model is obtained by adding Gaussian white-noise vectors to the deterministic model

$$\mathbf{x}(k+1)=\mathbf{F}_m(k)\cdot\mathbf{x}(k)+\mathbf{G}_m(k)\cdot E(k)+\mathbf{w}(k) \quad (18)$$

$$y(k)=\mathbf{C}\cdot\mathbf{x}(k)+\mathbf{v}(k). \quad (19)$$

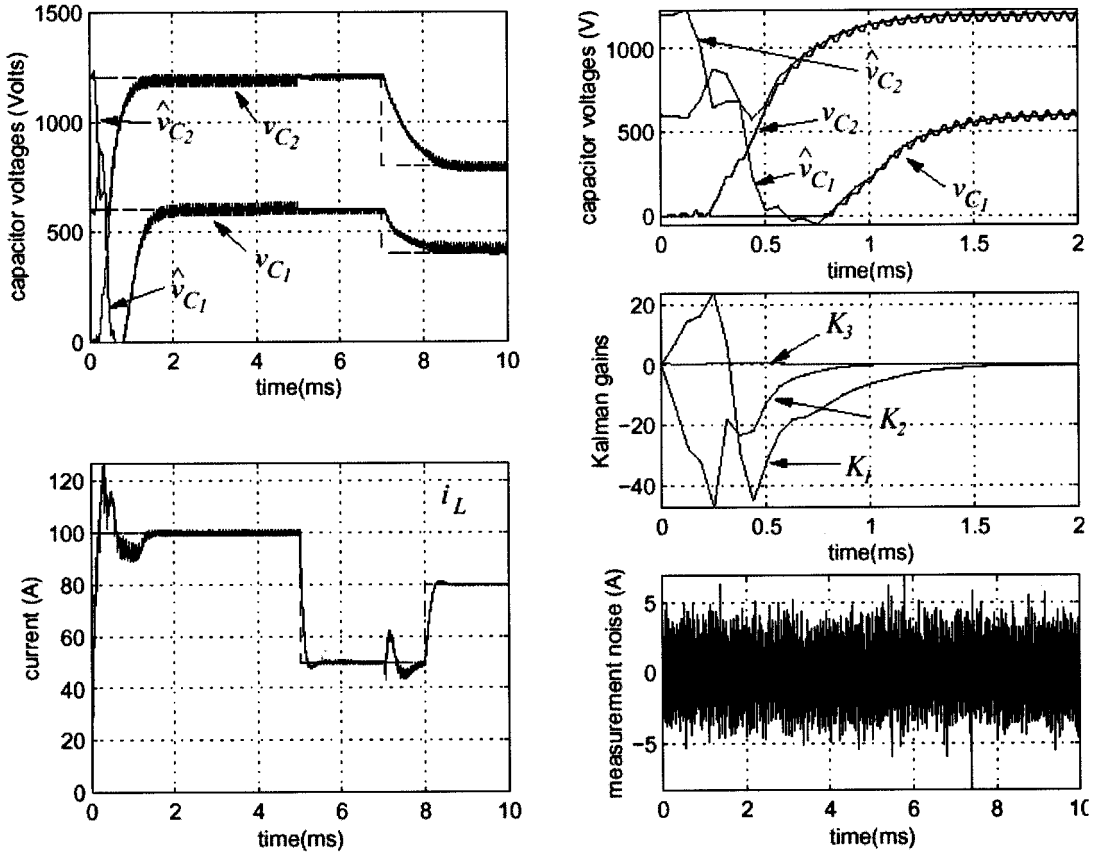

Fig. 15. Actual and observed states in the three-cell chopper. Linear state feedback decoupling control is used here. Simulation results.

The process noises $\mathbf{w}(k)$ and the measurement noises $\mathbf{v}(k)$ are characterized by

$$E\left\{\mathbf{w}(k)\mathbf{w}(i)^T\right\} = \begin{cases} \mathbf{Q}(k), & i = k \\ 0, & i \neq k \end{cases} \tag{20}$$

$$E\left\{\mathbf{v}(k)\mathbf{v}(i)^T\right\} = \begin{cases} R(k), & i = k \\ 0, & i \neq k \end{cases} \tag{21}$$

$$E\left\{\mathbf{w}(k)\mathbf{v}(i)^T\right\} = 0 \qquad \forall i \; et \; k \tag{22}$$

where $E\cdot$ denotes the expectation operator.

Taking into account the system noises, the KF algorithm will adapt the gains in order to minimize the trace of the error covariance matrix [15], [16].

The KF equations are as follows:

$$\mathbf{K}(k) = \mathbf{P}^{-}(k) \cdot \mathbf{C}^T \cdot \left(\mathbf{C} \cdot \mathbf{P}^{-}(k) \cdot \mathbf{C}^T + R(k)\right)^{-1} \tag{23}$$

$$\hat{\mathbf{x}}(k) = \hat{\mathbf{x}}^{-}(k) + \mathbf{K}(k) \cdot \left(y(k) - \mathbf{C} \cdot \hat{\mathbf{x}}^{-}(k)\right) \tag{24}$$

$$\mathbf{P}(k) = \mathbf{P}^{-}(k) - \mathbf{K}(k) \cdot \mathbf{C} \cdot \mathbf{P}^{-}(k) \tag{25}$$

$$\hat{\mathbf{x}}^{-}(k+1) = \mathbf{F}_m(k) \cdot \hat{\mathbf{x}}_k + \mathbf{G}_m(k) \cdot E(k) \tag{26}$$

$$\mathbf{P}^{-}(k+1) = \mathbf{F}_m(k) \cdot \mathbf{P}(k) \cdot \mathbf{F}_m(k)^T + \mathbf{Q}(k) \tag{27}$$

where $\mathbf{K}(\cdot)$ is the Kalman gain vector, $\hat{\mathbf{x}}(\cdot)$ is the state estimate, and the estimation error covariance is

$$\mathbf{P}(k) = E\left\{(\mathbf{x}(k) - \hat{\mathbf{x}}(k))(\mathbf{x}(k) - \hat{\mathbf{x}}(k))^T\right\}$$
$$\mathbf{P}^{-}(k) = E\left\{(\mathbf{x}(k) - \hat{\mathbf{x}}^{-}(k))(\mathbf{x}(k) - \hat{\mathbf{x}}^{-}(k))^T\right\}.$$

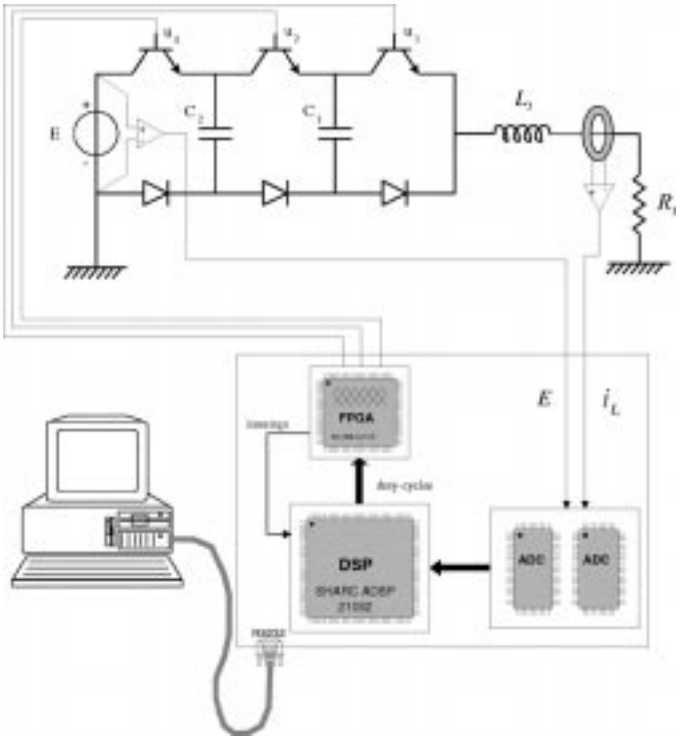

Fig. 16. DSP/FPGA-based sensorless control of the three-cell converter.

$\hat{\mathbf{x}}^{-}(k)$ denotes the prior estimate that represents our best estimate prior to assimilating the measurement $y(k)$, while $\hat{\mathbf{x}}(k)$

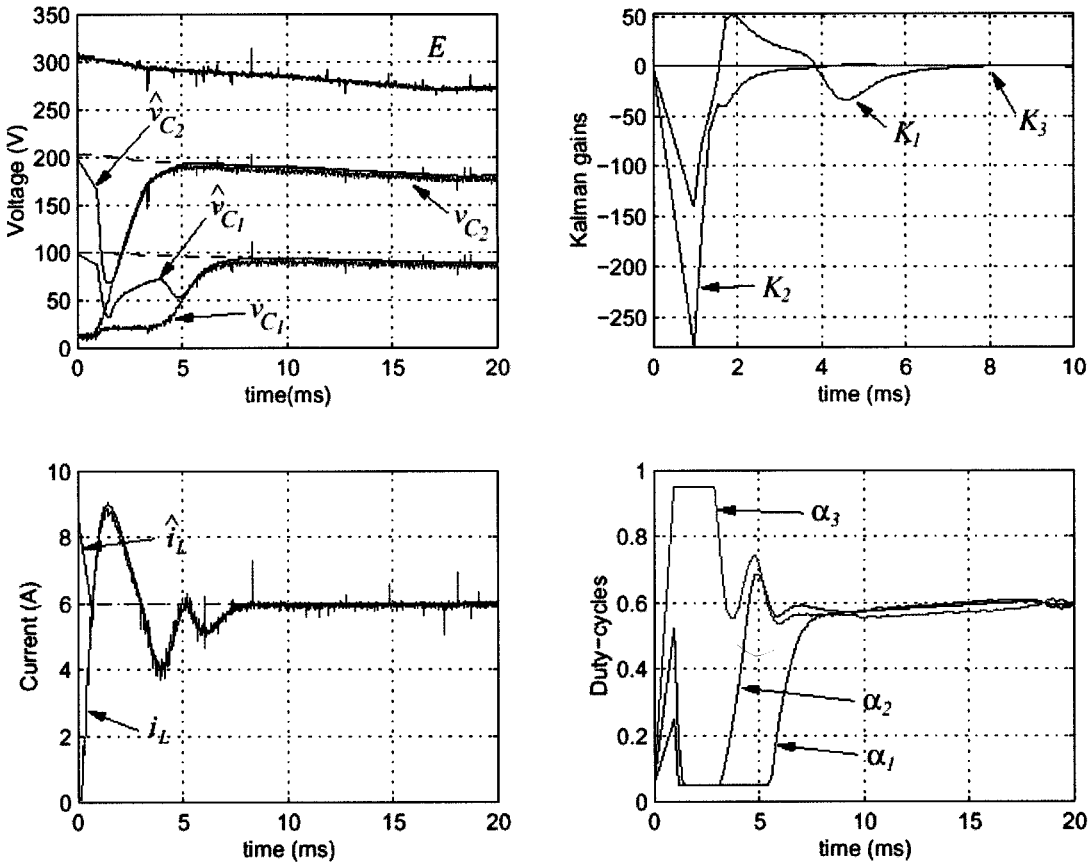

Fig. 17. Measured and estimated states when the converter starts with unknown initial conditions. Experimental results.

denotes the updated (or *a posteriori*) estimate after the measurement $y(k)$. $\mathbf{P}^{-}(k)$, and $\mathbf{P}(k)$ are, respectively, their associated error covariance matrices.

D. Capacitor Voltages Estimation

In this section, the application of the KF for the capacitor voltages estimation in a three-cell converter is presented. Since the model matrices depend on the duty cycles applied to the converter, the estimator is time varying and the Kalman gains must be evaluated online.

In the simulation results presented bellow, only a load current measurement is used for the capacitor voltages estimation. The supply voltage E must also be measured to impose the correct capacitor voltage references ($v_{C_1\text{ref}} = E/3$, $v_{C_2\text{ref}} = 2E/3$). The converter parameters are assumed to be known accurately and are given in (10). The current measurement has a Gaussian white noise added to account for imperfections in an experimental system. The measurement noise covariance is

$$R = 0.25A^2.$$

The process noise covariance is $\mathbf{Q} = 0.01 \cdot \mathbf{I}_3$ where $\mathbf{I}_3$ represents the 3×3 identity matrix.

Note that selection of the covariance matrices requires trials in practice and should be carried out with experimental data.

For the initial error covariance matrix $\mathbf{P}^{-}(0)$, an iterative research that yields the best estimation performance possible must be done.

In the following simulation, the best filter performance was obtained with

$$\mathbf{P}^{-}(0) = 5000 \cdot \mathbf{I}_3.$$

The simulation results are shown in Fig. 15 for a three-cell chopper when the algorithm starts with initial conditions different than the system initial conditions.

The estimates are used for a linear state feedback decoupling control strategy [19]. The control sequences used for this simulation are as follows:

- at $t = 0$ start of the converter with $E = 1800$ V and $i_{L\text{ref}} = 100$ A;
- at $t = 5$ ms step of the reference current of -50 A;
- at $t = 7$ ms step of the input voltage of -600 V;
- at $t = 8$ ms step of the reference current of 30 A.

We see that the estimated capacitor voltages are able to track the actual floating voltages quickly, even in the presence of measurement noises.

E. Real-Time Implementation and Experimental Results

In order to validate the simulation results, a test bench has been realized. The overall structure of the system is shown in Fig. 16. It contains a three-cell chopper, two analog sensors for source voltage measurement and current measurement, and an ADSP 21062 DSP system board including a XILINX 4010E field-programmable gate array (FPGA) and 14 A/D converters.

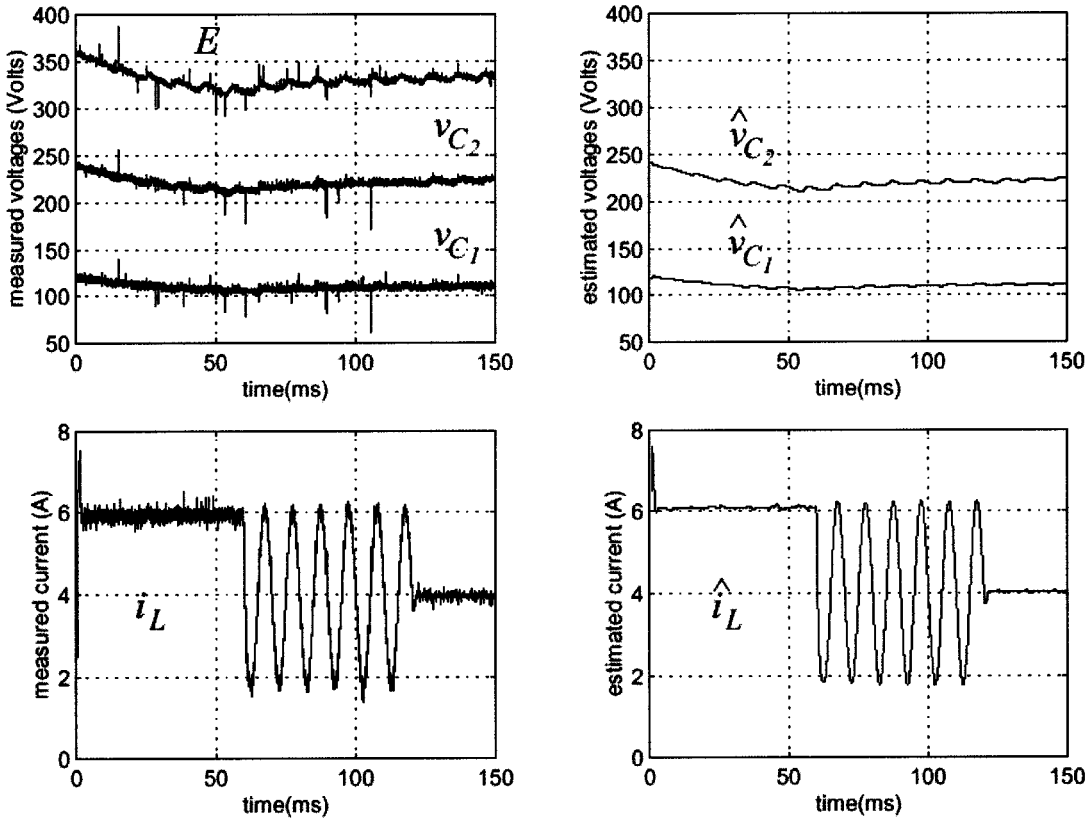

Fig. 18. Measured and estimated states in steady-state operation. Experimental results.

The DSP operates at 32 MHz and has a single cycle instruction of 31.25 ns. The PC is used to program the board (DSP/FPGA) and to communicate with the DSP in real time.

The DSP software contains the algorithm of the linear state feedback control strategy, the model calculations, and the recursive KF algorithm. The pulsewidth modulation (PWM) modulator is implemented in the FPGA. At the beginning of each switching period, the FPGA interrupts the DSP which starts the A/D conversions and executes the sensorless control algorithm. At the end of the algorithm the DSP writes the new duty-cycle values into the FPGA registers in order to be used by the modulator in the next switching period.

The converter parameters are as follows:

$$\begin{aligned} C_1 &= C_2 = 100\ \mu\text{F} \\ L_l &= 10\ \text{mH} \\ R_l &= 26\ \Omega \\ f_d &= 5.2\ \text{kHz}. \end{aligned}$$

The sampling and the switching frequencies are equal.

Two sets of experimental results are shown hereafter. Fig. 17 shows the results when the converter starts with discharged floating capacitors while the initial conditions for the observer are $\hat{\mathbf{x}}(0) = [100\ \text{V}, 200\ \text{V}, 10\ \text{A}]$..

In Fig. 18, experimental results are shown when the following control sequence is imposed:

$$\begin{cases} t < 0: & i_{L_{\text{ref}}} = 2\ \text{A} \\ 0 \le t < 60\ \text{ms}: & i_{L_{\text{ref}}} = 6\ \text{A} \\ 60\ \text{ms} \le t < 120\ \text{ms}: & i_{L_{\text{ref}}} = 4 - 2 \cdot \sin(2\pi f_m t) \\ & f_m = 100\ \text{Hz} \\ t \ge 120\ \text{ms}: & i_{L_{\text{ref}}} = 4\ \text{A}. \end{cases}$$

We see that the estimated and measured voltages are identical and the actual voltages are maintained at their optimal values: $E/3$ and $2E/3$.

V. Conclusions

Multicell converters are very interesting since they are suitable for high-power/high-voltage applications and considerably improve the output signal harmonics.

To take full advantage of this topology, the flying-capacitor voltages must be balanced to their optimal values ($E/3$ and $2E/3$ for a three-cell converter).

This objective can be achieved using a closed-loop control of the flying-capacitor voltages. A noninteractive control strategy based on an exact input–output linearization has been presented and experimentally validated.

In contrast to the passive control, the active control needs the knowledge of the converter states, especially the flying-capacitor voltages. In order to reduce the number of sensors in these converters and, consequently, the cost of the control system, the flying-capacitor voltages can be observed using only the load current measurement.

To achieve this purpose, the authors have proposed a novel model dedicated to observation based on state averaging techniques. This simple model allows the reduction of the required computational load and simplifies the real-time implementation of the observer.

Since the physical signals in the practice are noisy, a recursive KF has been adopted to take these random phenomena into account in the state estimation.

Simulation results show that the estimated voltages converge quickly toward the actual capacitor voltages, even in the presence of measurement noises. Experimental results obtained for a three-cell chopper confirm the usefulness of online estimation using a KF.

REFERENCES

[1] T. Meynard and H. Foch, "Multilevel choppers for high voltage applications," *EPE J.*, vol. 2, no. 1, pp. 45–50, Mar. 1992.

[2] ——, "Electronic device for electrical energy conversion between a voltage source and a current source by means of controllable switching cells," European Patent 92/916336.8, July 8, 1992.

[3] T. Meynard and M. Fadel, "Structure et commande des convertisseurs multicellulaires," presented at the Journées 3EI, Supélec, Gif sur Yvette, France, Mar. 20–21, 1997.

[4] T. Meynard, M. Fadel, and N. Aouda, "Modeling of multilevel converters," *IEEE Trans. Ind. Electron.*, vol. 44, pp. 356–364, June 1997.

[5] G. Gateau, "Contribution à la commande des convertisseurs statiques multicellulaires: Commande non linéaire et commande floue," Ph.D. dissertation, INP, Toulouse, France, 1997.

[6] R. Bensaid, M. Fadel, and T. Meynard, "Observer design for a three-cell chopper using a discrete-time model," in *Proc. ELECTROMOTION*, Patras, Greece, 1999, pp. 689–694.

[7] T. Meynard, M. Fadel, and N. Aouda, "Modeling of multilevel converters," *IEEE Trans. Ind. Electron.*, vol. 44, pp. 356–364, June 1997.

[8] P. Carrere, "Convertisseurs multicellulaires," Ph.D. dissertation, INP, Toulouse, France, 1996.

[9] P. Carrere, T. Meynard, and J. P. Lavieville, "4000V-300A eight level IGBT inverter leg," in *Proc. EPE'95*, Seville, Spain, 1995, pp. 106–111.

[10] D. Pinon, M. Fadel, and T. Meynard, "Sliding mode control for a two-cell chopper: Study of the convergence to limit cycle," *Rev. Int. Gen. Elect.*, vol. 1, no. 3, pp. 393–415, Sept. 1998.

[11] J. J. Slotine and W. Li, *Applied Nonlinear Control*. Englewood Cliffs, NJ: Prentice-Hall, 1989.

[12] H. Sira-Ramirez and M. Ilic-Spong, "Exact linearization in switched mode DC to DC power converter," *Int. J. Control*, no. 50, pp. 511–524, 1989.

[13] A. Oukaour, J. P. Barbot, and B. Pioufle, "Non linear control of a variable frequency DC-DC converter," in *Proc. IEEE Conf. Control Applications*, Glasgow, U.K., 1994, pp. 499–500.

[14] R. Bensaid and M. Fadel, "Flying voltages estimation in three-cell converters using a discrete-time Kalman filter," presented at the IEEE PESC, Vancouver, BC, Canada, June 17–21, 2001.

[15] R. G. Brown and P. Y. C. Hwang, *Introduction to Random Signals and Applied Kalman Filtering*. New York: Wiley, 1997.

[16] A. Gelbal *et al.*, *Applied Optimal Estimation*. Cambridge, MA: MIT Press, 1974.

[17] A. J. Fossard and D. Normant-Cyrot, *Systèmes Non Linéaires*. Paris, France: Masson, 1993.

[18] S. Cuk and R. D. Middelbrook, "A general unified approach to modeling switching converters power stages," in *Proc. IEEE PESC'76*, 1976, pp. 18–34.

[19] O. Tachon, M. Fadel, and T. Meynard, "Control of series multicell converters by linear state feedback decoupling," in *Proc. EPE'97*, 1997, pp. 1.588–1.593.

Guillaume Gateau graduated from the Ecole Normale Supérieure de Cachan, Cachan, France, in 1992, and received the Ph.D. degree from the Institut National Polytechnique de Toulouse, Toulouse, France, in 1997.

In 1998, he joined the Laboratoire d'Electrotechnique et d'Electronique Industrielle (LEEI), Institut National Polytechnique de Toulouse/Centre National de la Recherche Scientifique, Toulouse, France, as an Assistant Professor. His research interests include digital control of power converters, series multicell converters for high-power and high-performance applications, and new topologies for high-voltage applications.

Maurice Fadel was born in Toulouse, France, in 1958. He received the Doctorate degree from the Institut National Polytechnique de Toulouse, Toulouse, France, in 1988.

He is currently a Professor in the Ecole Nationale d'Electrotechnique d'Electronique d'Informatique et d'Hydraulique de Toulouse, Toulouse, France. In 1985, he joined the Laboratoire d'Electrotechnique et d'Electronique Industrielle (LEEI), Institut National Polytechnique de Toulouse/Centre National de la Recherche Scientifique, Toulouse, France. His work concerns the modeling and control of electric systems. He is currently the Head of Control Group in the LEEI. This group is comprised of ten researchers in the field of electrical control. He has authored numerous published technical papers.

Pascal Maussion received the Ph.D. degree from the Institut National Polytechnique de Toulouse, Toulouse, France, in 1990.

Since 1990. he has been a Researcher in the Laboratoire d'Electrotechnique et d'Electronique Industrielle, Institut National Polytechnique de Toulouse/Centre National de la Recherche Scientifique, Toulouse, France. His research activities deal with fuzzy control of electrical and mechanical systems, with nonlinear control of power converters, genetic algorithms for optimization in power electronics, and control laws for soft switching.

Rédha Bensaid was born in Algiers, Algeria, in 1972. He received the B.Sc. degree from the Ecole Nationale Polytechnique of Algiers, Algiers, Algeria, in 1994, and the M.Sc. and Ph.D. degrees from the Institut National Polytechnique de Toulouse, Toulouse, France, in 1997 and 2001, respectively, all in electrical engineering.

He is currently a Post-Doctoral Fellow in the Laboratoire d'Electrotechnique et d'Electronique Industrielle, Institut National Polytechnique de Toulouse/Centre National de la Recherche Scientifique, Toulouse, France, working in the area of active power filters. His fields of interest are power electronics, drives, sensorless control, power quality, and digital signal processing.

Thierry A. Meynard (M'94) graduated from the Ecole Nationale Supérieure d'Electrotechnique, d'Electronique, et d'Hydraulique de Toulouse, Toulouse, France, in 1985, and received the Ph.D. degree from the Institut National Polytechnique de Toulouse, Toulouse, France, in 1988.

He was an Invited Researcher at the Université du Québec á Trois Riviéres, Canada, in 1989. He joined the Laboratoire d'Electrotechnique et d'Electronique Industrielle (LEEI), Institut National Polytechnique de Toulouse/Centre National de la Recherche Scientifique, Toulouse, France, as a full-time Researcher in 1990. He was Head of the Static Converter Group at LEEI from 1994 to 2001, and is currently Directeur de Recherches. He is also a part-time Consultant with Cirtem. His research interests include soft commutation, series and parallel multicell converters for high-power and high-performance applications, and direct ac/ac converters.

His research interests include soft-commutation, series and parallel multicell converters for high power and high performance applications and direct AC/AC converters.